

# Some effects of small-scale metallicity variations in cooling flows

R. Glenn Morris<sup>\*</sup> and A. C. Fabian

*Institute of Astronomy, Madingley Road, Cambridge CB3 0HA*

3 September 2018

## ABSTRACT

In an attempt to reconcile recent spectral data with predictions of the standard cooling flow model, it has been suggested that the metals in the intracluster medium (ICM) might be distributed inhomogeneously on small scales. We investigate the possible consequences of such a situation within the framework of the cooling flow scenario. Using the standard isobaric cooling flow model, we study the ability of such metallicity variations to preferentially suppress low-temperature line emission in cooling flow spectra. We then use simple numerical simulations to investigate the temporal and spatial evolution of the ICM when the metals are distributed in such a fashion. Simulated observations are used to study the constraints real data can place on conditions in the ICM. The difficulty of ruling out abundance variations on small spatial scales with current observational limits is emphasized. We find that a bimodal distribution of metals may give rise to interesting effects in the observed abundance profile, in that apparent abundance gradients with central abundance drops and off-centre peaks, similar to those seen recently in some clusters, are produced. Different elements behave in different fashion as governed by the temperature dependence of their equivalent widths. Our overall conclusion is that, whilst this process alone seems unlikely to be able to account for the sharp reduction in low temperature emission lines seen in current spectral data, a contribution at some level is possible and difficult to rule out. The possibility of small-scale metallicity variations should be considered when analysing high resolution cluster X-ray spectra.

**Key words:** cooling flows – galaxies: abundances – galaxies: clusters: general – X-rays: galaxies

## 1 INTRODUCTION

Data from the latest generation of X-ray satellites, *Chandra* and *XMM-Newton*, are forcing us to re-examine some of the basic tenets of the traditional cooling flow model (e.g., Fabian 1994). Various authors (e.g., Kaastra et al. 2001; Peterson et al. 2001; Tamura et al. 2001) have drawn attention to the discrepancy between the predictions of the standard cooling flow model and observed spectra of cluster central regions. The expected emission lines for several important species (e.g. the Fe XVII 15 and 17 Å lines) do not seem to be present at the levels which simple models would expect. This is a trend that appears to be repeated in many clusters that have traditionally been thought to harbour cooling flows (Peterson et al. 2002). Lines such as these are important because they are strong indicators of low ( $\lesssim 1$  keV) temperature gas (see Section 2.1). In a standard cooling

flow, in which gas is cooling down to essentially zero, we expect a significant flux in such lines.

Several ideas (e.g., Fabian et al. 2001; Peterson et al. 2001) have been put forward to explain this discrepancy. Here we focus on just one of these, the suggestion that the intracluster medium (ICM) metals might be distributed inhomogeneously on small-scales. We examine in detail the consequences of such a scenario, investigating the effects of an ICM metallicity which varies on small, unresolved scales (sub-kpc, say). This idea is no more than a minor extension of the multiphase cooling flow model (Nulsen 1986), which has always relied upon the coexistence of phases with different densities and temperatures at the same radius in the ICM. We merely allow the chemical composition of these phases to vary as well. This idea is attractive in the context of cooling flows since it leaves the spectra of high ( $\gtrsim 1$  keV) temperature gas essentially unchanged, whilst reducing the line emission from low temperature gas. It (potentially) enables us to reconcile the data and models whilst making the smallest conceptual changes to the standard model.

<sup>\*</sup> E-mail: gmorris@ast.cam.ac.uk

Indeed, given that a suppression of thermal conduction (electron motion) implies an even more severe reduction in the freedom of heavy ions to diffuse through the ICM, we might expect small-scale metallicity variations to be a natural consequence of the multiphase cooling flow model, in which conduction is by necessity heavily reduced. Conversely, if ICM thermal conduction is relatively efficient (as has been suggested recently by several authors, e.g., Narayan & Medvedev 2001; Voigt et al. 2002) then this does not necessarily imply that the same is true of ion motion.

In Section 2 we examine the effects of an inhomogeneous metallicity within the framework of the standard isobaric cooling flow model (e.g., Johnstone et al. 1992), quantifying the reduction in equivalent width that can be expected for several important ICM species as the degree of inhomogeneity is varied. In Section 3 we outline an improved numerical model that allows us to carry out simulations with spatial and temporal evolution, and to produce simulated observations of *Chandra* spectral data. Section 4 describes some of the results of this model for a simple case of metallicity inhomogeneities. We find that small-scale abundance variations may give rise to the appearance of abundance gradients where none in fact exist, with the results for individual species being controlled by the temperature dependence of their equivalent widths. We stress the difficulty of resolving such variations without a combination of good spatial and spectral resolution. In the final Section we make some discussion concerning the likelihood of such small-scale metallicity variations in the ICM. Given that direct detection of such structures is currently unfeasible, we put forward some suggestive circumstantial evidence.

Throughout this paper we assume:  $H_0 = 50 \text{ km s}^{-1} \text{ Mpc}^{-1}$ ;  $\Omega_M = 1.0$ ,  $\Omega_\Lambda = 0.0$ . We make use of XSPEC version 11.

## 2 COOLING FLOW SPECTRA

### 2.1 ICM thermometers

Fig. 1a shows the temperature dependence of the equivalent width of the  $15 \text{ \AA}$  Fe XVII line, for various metallicities, for a single temperature plasma, as calculated using the MEKAL plasma code (Mewe et al. 1995; Kaastra & Mewe 1993). This code computes the bremsstrahlung continuum and line radiation from a plasma (of up to 15 elements) in the coronal equilibrium approximation (e.g., Brickhouse et al. 1995) over the temperature range  $10^4$ – $10^9$  K. The equivalent width curves are sharply peaked around 0.3 keV ( $\sim 10^6$  K), so these emission lines are sensitive indicators of gas at such temperatures. Furthermore, they are extremely strong – Fig. 1b shows the fraction of the power (in the X-ray waveband 0.1–10.0 keV) being emitted at any temperature in this iron line. For a solar metallicity plasma, it peaks around the 10 per cent level. The results are similar for the  $17 \text{ \AA}$  line. Consequently, these lines are highly important coolants below 1 keV, and therefore in the standard cooling flow model (in which gas cools from a temperature of several keV to essentially zero), we expect a strong flux in these lines. The actual fluxes seen in many cooling flow clusters are much weaker than would be expected (e.g., Kaastra et al. 2001; Peterson et al. 2001; Tamura et al. 2001).

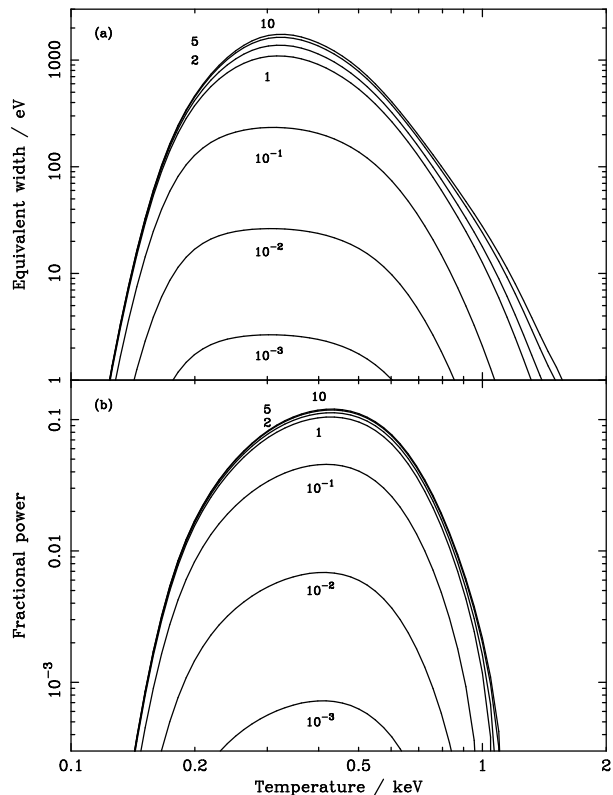


**Figure 1.** Behaviour of the Fe XVII  $15.0 \text{ \AA}$  line in a coronal equilibrium single temperature plasma. The curve labels refer to metallicity in solar units. The top panel shows the equivalent width in eV, the bottom panel shows the fractional power (in the X-ray waveband 0.1–10.0 keV) contained in this line.

### 2.2 Bimodal metallicities

#### 2.2.1 Fixed temperature plasmas

Several ideas (e.g., Fabian et al. 2001; Peterson et al. 2001) have been put forward to explain this missing low temperature flux. Here we focus on just one of these, the suggestion that the ICM metals might be inhomogeneously distributed on small-scales. The essence of this idea is as follows. At any fixed single temperature, a two-component plasma consisting of metal-rich and metal-poor ‘phases’ (note that the usage of the term phase here is not necessarily strictly the same as in traditional multiphase cooling flow models) is spectroscopically indistinguishable from a homogeneous plasma of some mean metallicity  $\bar{Z} = f_{\text{hi}} Z_{\text{hi}} + (1 - f_{\text{hi}}) Z_{\text{lo}}$ , where the metal-rich phase has a metallicity  $Z_{\text{hi}}$  and accounts for a mass fraction  $f_{\text{hi}}$ , and the metal-poor phase has a metallicity  $Z_{\text{lo}}$ . For simplicity (and without loss of generality), we take  $Z_{\text{lo}} \equiv 0$ .  $f_{\text{hi}} = 1$  corresponds to a uniform plasma, and decreasing values of  $f_{\text{hi}}$  to increasingly segregated plasmas. Throughout this paper, we leave the He abundance fixed at the solar value, allowing the heavy elements to vary as specified by  $Z$ . We use the solar abundance ratios of Anders & Grevesse (1989), hereinafter  $Z_\odot$ .

The indistinguishability of the spectra in these two cases

is a simple consequence of the fact that the strength of the continuum radiation is independent of  $Z$ , whilst that of the emission lines is directly proportional to  $Z$ . The reduction in the mass fraction of the enriched phase is therefore offset by the increased line strength. Alternatively, in the coronal limit, the local concentration of the heavy elements makes no difference to their radiation: a given number of heavy ions will radiate in the same way whether uniformly dispersed throughout the emitting volume or concentrated in a specific region. As an aside, we note that this simplistic treatment breaks down at very high metallicities ( $Z \gtrsim 70 Z_\odot$ ) when the free electrons contributed by the metal ions become significant. This would not invalidate the idea that a mixture of a metal-rich and a metal-poor plasma can look identical to a uniform metallicity plasma, it would merely change the dependence of the normalization of each component on  $Z$  from a simple linear relationship to something more complicated. Such ultra-high metallicities are of no relevance here though.

### 2.2.2 Cooling plasmas

The situation becomes more complex when one allows cooling to occur. We briefly review the derivation of the standard isobaric cooling flow model (e.g., Johnstone et al. 1992). The energy released per unit mass of gas on cooling by  $dT$  is

$$\begin{aligned} dq &= du + pd \left( \frac{1}{\rho} \right) = d \left( u + \frac{p}{\rho} \right) \quad (\text{constant } p) \\ &= d \left( \frac{3}{2} \frac{k_B T}{\mu m_H} + \frac{n k_B T}{\rho} \right) \quad (\text{ideal gas}). \end{aligned}$$

For a constant mass-flow rate  $\dot{M}$ , the power release is thus

$$dL = \frac{5}{2} \frac{k_B}{\mu m_H} \dot{M} dT. \quad (1)$$

We also have, from the definition of the cooling function  $\Lambda$ ,

$$\begin{aligned} dL &= n_e n_H \Lambda(T, Z) dV, \\ dL_\nu &= n_e n_H \Lambda_\nu(T, Z) dV. \end{aligned} \quad (2)$$

Hence we obtain the spectral power for a steady-state flow cooling from  $T_{\max}$  to  $T_{\min}$

$$L_\nu = \frac{5}{2} \frac{k_B}{\mu m_H} \dot{M} \int_{T_{\min}}^{T_{\max}} \frac{\Lambda_\nu(T, Z)}{\Lambda(T, Z)} dT. \quad (3)$$

Thus, we have the simple result that the emission measure of each temperature component in the flow is inversely proportional to the cooling function  $\Lambda(T)$  at that temperature. This model is implemented by the XSPEC package as the `mkcflow` and `vmcflow` models<sup>1</sup>. We have constructed an independent implementation of Eqn. 3, calculating cooling

<sup>1</sup> We draw attention to the fact that in the XSPEC `mkcflow` implementation, altering the plasma bulk metallicity varies the helium abundance (for XSPEC versions prior to 11.1.0ab). This can have a non-negligible effect on the calculation of equivalent widths when high metallicities are involved. As a workaround, the `vmcflow` model may be used to specify abundances on an element-by-element basis.

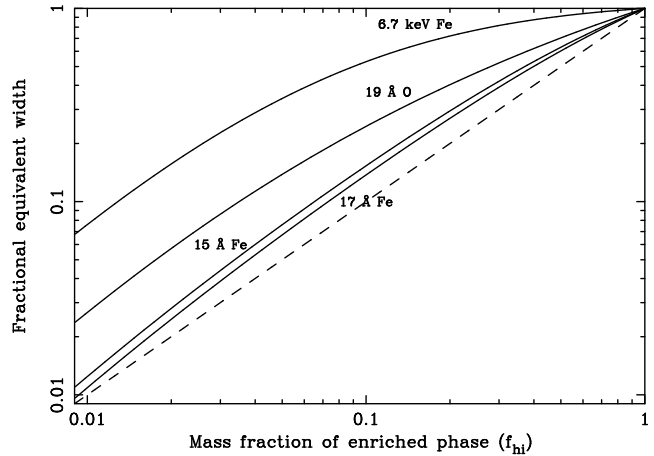


**Figure 2.** Fractional change in the equivalent width of some important emission lines from the cooling flow model of Eqn. 3, for two-component plasmas, as the mass fraction of the enriched phase is varied. The dashed line is the reference line  $y = x$ . Parameters of the cooling flow model:  $\bar{Z} = 0.3 Z_\odot$ ,  $Z_{\text{lo}} \equiv 0$ ,  $Z_{\text{hi}} = f_{\text{hi}}^{-1} \bar{Z}$ . The integration over temperature was performed at 100 points, logarithmically spaced between 0.0808–8.620 keV.

functions by integrating MEKAL spectra against energy over the 5 eV–200 keV range.

The heating solutions to the cooling flow spectral problem (i.e. the absence of spectral lines characteristic of cool,  $\lesssim 1$  keV, gas) suppress the low-temperature line emission by raising  $T_{\min}$  to  $\sim 1$  keV. The bimodal metallicity hypothesis suppresses the equivalent width (EW) of the low-temperature lines by a different means. In Fig. 2 we illustrate how the EW of various important spectral features changes as a function of  $f_{\text{hi}}$  (or  $Z_{\text{hi}}$ ), for the case  $\bar{Z} = 0.3 Z_\odot$ . The dashed line shows what might be the naive expectation, namely that  $\text{EW}(f_{\text{hi}}) = f_{\text{hi}} \text{EW}(1)$ . In no case is this line followed – the reduction in the EW is always less than this. Thus, for example, at  $f_{\text{hi}} = 0.1$ , the EW of the Fe K $\alpha$  line is reduced by a factor of about 0.5, that of the 19 Å O line by about 0.25, and that of the 15 Å Fe line by around 0.15. We can interpret these results as follows.

Recall the definition of equivalent width

$$\text{EW} \equiv \int_{E_0}^{E_1} \frac{I_{\text{L+C}} - I_{\text{C}}}{I_{\text{C}}} dE, \quad (4)$$

where  $I_{\text{L+C}}$  is the total (line + continuum) intensity at a given energy, and  $I_{\text{C}}$  is the continuum intensity at the same point.

For fixed, narrow line profiles, we can neglect the integral over energy and simply compare intensity ratios at the line energy. Making use of the cooling flow equation Eqn. 3, we may write the equivalent width,  $\text{EW}(H)$ , for a given spectral line (with a narrow energy profile centred on some energy  $E$ ) from a homogeneous metallicity cooling flow as

$$\text{EW}(H) = \frac{\int_{T_{\min}}^{T_{\max}} \frac{\Lambda_{\text{L}}(T, E, \bar{Z})}{\Lambda(T, \bar{Z})} dT}{\int_{T_{\min}}^{T_{\max}} \frac{\Lambda_{\text{C}}(T, E, \bar{Z})}{\Lambda(T, \bar{Z})} dT}. \quad (5)$$

In this expression,  $\Lambda_L n_e n_H$  would be the power per unit volume per unit energy radiated by the line component at a given energy, with  $\Lambda_C$  having an analogous meaning for the continuum component. Integrating the sum of these two functions over energy leads to the cooling function  $\Lambda(T, Z)$ .

For a two-component ('bimodal') cooling flow, in which one component has a metallicity  $Z_{\text{hi}}$  and accounts for a fraction  $f_{\text{hi}}$  of the total mass flow rate, and the other component has zero metals, we have the following expression for the equivalent width,  $\text{EW}(B)$ , of a narrow spectral line centred at energy  $E$ :

$$\text{EW}(B) = f_{\text{hi}} \int_{T_{\text{min}}}^{T_{\text{max}}} \frac{\Lambda_L(T, E, Z_{\text{hi}})}{\Lambda(T, Z_{\text{hi}})} dT \quad / \quad \left\{ \int_{T_{\text{min}}}^{T_{\text{max}}} \left[ f_{\text{hi}} \frac{\Lambda_C(T, E, Z_{\text{hi}})}{\Lambda(T, Z_{\text{hi}})} + (1 - f_{\text{hi}}) \frac{\Lambda_C(T, E, 0)}{\Lambda(T, 0)} \right] dT \right\}. \quad (6)$$

Our desire is to suppress the equivalent width of the low-temperature lines in the bimodal case – that is, the ratio of Eqn. 6 to Eqn. 5 should be  $< 1$  in such cases. There exists no simple algebraic solution to this form, owing to the non-analytic behaviour of the  $\Lambda$  functions.

Restricting our attention to an emission line that exists only over a narrow temperature range (for example, the Fe XVII 15 Å line, as illustrated in Fig. 1), however, we may make the simplification  $\int \frac{\Lambda_L(T)}{\Lambda(T)} dT \rightarrow \frac{\Lambda_L(\bar{T})}{\Lambda(\bar{T})} \delta T$ . In addition, we have the result that  $\Lambda_L n_e n_H \propto n_e n_{\text{ion}} \Rightarrow \Lambda_L \propto n_{\text{ion}} \propto Z$  (at fixed  $n_H$ ). Consequently

$$\frac{\Lambda_L(\bar{T}, E, Z_{\text{hi}})}{\Lambda_L(\bar{T}, E, \bar{Z})} = \frac{Z_{\text{hi}}}{\bar{Z}} = \frac{1}{f_{\text{hi}}}. \quad (7)$$

The ratio of the equivalent widths may therefore be somewhat simplified to

$$\frac{\text{EW}(B)}{\text{EW}(H)} = \frac{\Lambda(\bar{T}, \bar{Z})}{\Lambda(\bar{T}, Z_{\text{hi}})} \int_{T_{\text{min}}}^{T_{\text{max}}} \frac{\Lambda_C(T, E, \bar{Z})}{\Lambda(T, \bar{Z})} dT \quad / \quad \left\{ \int_{T_{\text{min}}}^{T_{\text{max}}} \left[ f_{\text{hi}} \frac{\Lambda_C(T, E, Z_{\text{hi}})}{\Lambda(T, Z_{\text{hi}})} + (1 - f_{\text{hi}}) \frac{\Lambda_C(T, E, 0)}{\Lambda(T, 0)} \right] dT \right\}. \quad (8)$$

The term involving the ratio of integrals is the ratio of the continuum in the homogeneous case to that in the bimodal case. By inspection of cooling flow spectra, this ratio is very close to one. Most of the continuum flux is contributed by gas at temperatures  $\gtrsim 1$  keV, where the metals have relatively little influence on the cooling function. Bimodal plasmas tend to have fractionally stronger continua at low ( $\lesssim 1$  keV) energies, where low-temperature gas makes a slight contribution. The reduced cooling function of the low-metallicity phase at low temperatures enhances its emission measure compared to the mean metallicity case.

In the idealized case of a narrow emission line, the ratio of the equivalent widths for the two cases therefore reduces to the ratio of the cooling functions  $\Lambda(\bar{T}, \bar{Z})/\Lambda(\bar{T}, Z_{\text{hi}})$ . For a high-temperature ( $\gtrsim 1$  keV) line, where cooling is essentially independent of metallicity, the ratio of the equivalent widths reduces to one. For a low-temperature line, then if the metals were to completely dominate the cooling, we expect the ratio to reduce to  $\bar{Z}/Z_{\text{hi}} = f_{\text{hi}}$ .

Qualitatively, on increasing the metallicity by a factor  $f_{\text{hi}}^{-1}$ , the emission line strength (at all temperatures) increases proportionately. Reducing the mass fraction compensates, so that spectra at any fixed temperature are un-

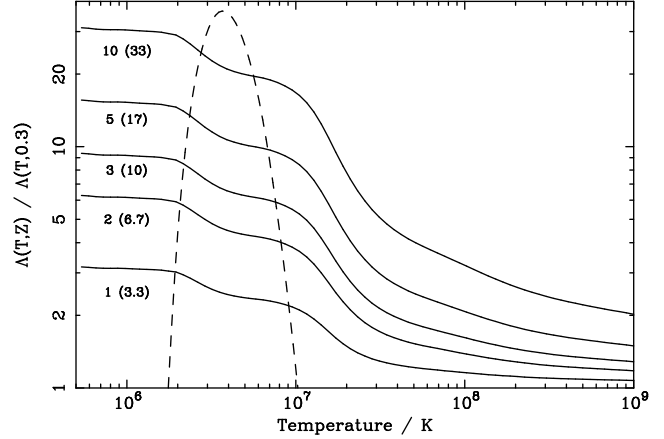


**Figure 3.** Dependence of the cooling function  $\Lambda(T)$  on metallicity. The labelled curves show the cooling function for a given metallicity (in solar units) relative to that for  $0.3 Z_{\odot}$ . The numbers in parentheses are the metallicities as multiples of  $0.3 Z_{\odot}$ . At low temperatures, the curves asymptote out to these values. Above  $10^8$  K the cooling is dominated by the H, He continuum; as the temperature decreases to  $\sim 10^6$  K Fe becomes increasingly dominant; and towards the end of the range O is the major coolant. The dashed curve shows the equivalent width of the Fe XVII 15 Å line in arbitrary units.

changed. When steady-state cooling is allowed to take place, however, the faster cooling of the metal-rich gas at low temperatures reduces its emission measure and suppresses its spectral contribution.

The cooling function ratio is plotted for some representative metallicities in Fig. 3. Note that metals do not fully dominate the cooling function until  $T \lesssim 10^6$  K. In the temperature range where the Fe XVII 15 Å line is strong (overlaid), the ratio of the cooling function for  $Z = 3.0 Z_{\odot}$  to that for  $Z = 0.3 Z_{\odot}$  is in the range 6–7. This is consistent with the result from Fig. 2 for this line with  $f_{\text{hi}} = 0.1$ , where a fractional suppression of the EW of order 0.15 is found. This is to be contrasted with the simple expectation of 0.1. The actual suppression of this line is not so strong.

In practice for lines existing at intermediate temperatures, or over a non-negligible range of temperatures, we expect behaviour between these limits. The iron K line, for example, deriving as it does from gas over a relatively wide, high temperature range (see Fig. 8), has its equivalent width suppressed by about a factor of 0.5, for  $f_{\text{hi}} = 0.1$ . If this were the case, then analyses not taking this into account would have underestimated the mean ICM metallicity. As another consequence of this, the *relative* suppression of the Fe XVII line (say) compared to that of the Fe K line, is only a factor of 0.3. In other words, given a spectrum of unknown metallicity, if one were to fit an abundance from the iron K line, then attempt to reproduce the observed Fe XVII line with this abundance, the observed line would be about a factor of three smaller than predicted. This is of course appreciably less than the simple ‘factor of ten’ reduction that might have been expected. Consequently, it seems unlikely that small-scale metallicity variations alone can be responsible for the very strong suppression of the equivalent widths of low-temperature emission lines seen in cooling flow spec-

tra, unless the range of the variations were to be pushed to extreme levels.

$f_{\text{hi}} = 0.1$  corresponds to  $f_{\text{hi}} \approx 3 Z_{\odot}$ . This may seem like an excessively high metallicity, but consider that supernovae can be viewed as sources of essentially infinite metallicity. The *Chandra* observation (Iwasawa et al. 2001) of 4C55.15 reveals a metallicity  $\approx 2 Z_{\odot}$  within the central 50 kpc, as well as a metal-rich ‘plume’ extending over  $\sim 25$  kpc with  $Z \approx 8 Z_{\odot}$ . Whilst this is clearly an extreme case, if such high-metallicity features can be produced on these scales, there is no reason they cannot occur on the much smaller scales we consider.

### 3 AN IMPROVED COOLING FLOW MODEL

The standard isobaric cooling-flow model represented by Eqn. 3 is a useful tool, but it suffers from a number of limitations. It assumes a constant pressure, and is inherently single-phase. It assumes a steady-state with no time dependence. Furthermore, there is no spatial information, and no attempt to treat the gravitational potential of the cluster. It is a good first approximation to the global properties of a cooling flow, but in the new era of high spatial resolution X-ray spectroscopy and imaging, being able to study the temporal and spatial evolution of the ICM becomes more and more desirable. An improved model may be obtained by following the numerical prescription of Thomas (1988). The underlying theoretical basis is that of Nulsen (1986). We assume spherical symmetry, so that the system can be described by a one-dimensional model.

#### 3.1 The dark matter

We simulate a cluster simply as a two-component system, comprised of hot gas in the potential well of a dark matter (DM) halo. We represent the latter by a standard Navarro, Frenk and White (NFW) profile (Navarro et al. 1997). In order to specify the parameters of the profile, we make use of the calibrated virial scaling relations of Evrard et al. (1996):

$$\begin{aligned} M(r_{200}) &= 2.9 \times 10^{15} h_{50}^{-1} \left( \frac{T}{10 \text{ keV}} \right)^{\frac{3}{2}} M_{\odot}, \\ r_{200}(T) &= 3.7 h_{50}^{-1} \left( \frac{T}{10 \text{ keV}} \right)^{\frac{1}{2}} \text{ Mpc}; \end{aligned} \quad (9)$$

where  $r_{200}$  is the radius at which the density contrast (i.e. density in units of the critical density) is equal to 200, and serves to define a virial radius for the cluster (e.g., Cole & Lacey 1996). We complete the specification of the DM profile by taking a typical cluster value of 5 (e.g., Bullock et al. 2001) for the concentration parameter (i.e. the virial radius in units of the NFW scale radius).

#### 3.2 The gas

The gas is modelled as a single-phase medium. The traditional assumption for cooling flows has been that the unstable nature of the cooling process would lead to a highly multiphase medium (e.g., Allen 2000), i.e. phases of different densities and temperatures coexist at the same radius.

Recent observations cast doubt on this assumption, though – see for example Molendi & Pizzolato (2001).

For initial conditions, we assume a continuous smooth pressure profile of the isothermal form, normalized in terms of an (initially arbitrary) outer boundary pressure at the virial radius. The gas is assigned a density profile which is proportional to the pressure profile. The scaling is such that the temperature of the gas at the outer boundary is equal to the virial temperature of the cluster. Note that when we allow the metallicity of the gas to vary spatially, the molecular weight  $\mu$  is not constant, and we calculate the outer boundary temperature using a ‘mean’  $\mu$ . Also, in such cases the gas will not be isothermal, since for a smooth pressure profile to exist, regions of high  $\mu$  must be at higher temperatures.

The total mass of gas is calculated via numerical integration of the density profile. We adjust the outer boundary pressure so that the system gas mass corresponds to some appropriate fraction  $f_{\text{gas}}$  of the total (gas plus DM) mass. A temperature profile  $T(r)$  may then be assigned using the (ideal gas) equation of state.

#### 3.3 Evolution of the system

The system is allowed to evolve under the influence of gravity (neglecting the gas self-gravity) and radiative energy loss. We simulate the cluster over the radial range  $0 < r < r_{200}$ , i.e. out to the virial radius. For boundary conditions, we impose a stationary inner boundary and a constant pressure outer boundary. The latter is acceptable because unphysically long time-scales would be required for the effects of cooling to propagate out as far as the virial radius. The governing differential equations are represented by the Lagrangian difference scheme of Thomas (1988). Put simply, the radial range is divided into a large number of zones, which are then evolved forward in discrete time-steps. We use an adaptive step-size that is limited by stability considerations, but also by the cooling time of the gas, which in the standard isobaric assumption is given by

$$t_{\text{cool}} = \frac{\gamma}{\gamma - 1} \left( \frac{k_{\text{B}}}{\mu X_{\text{H}}} \right)^2 \frac{1}{e_{\text{r}} p} \int_0^T \frac{T \text{ d}T}{\Lambda(T)}, \quad (10)$$

where:  $\gamma$  is the adiabatic index of the plasma;  $X_{\text{H}} = n_{\text{H}} m_{\text{H}} / \rho$  is the hydrogen mass fraction;  $e_{\text{r}} = n_{\text{e}} / n_{\text{H}}$  is the electron density relative to the hydrogen density. With the cooling function  $\Lambda(T) \sim T^{\frac{1}{2}}$  (at high temperatures) for bremsstrahlung, then at a fixed pressure  $t_{\text{cool}} \sim T^{\frac{3}{2}}$ ; whereas for virially-scaled clusters with  $p \propto T$  at a fixed overdensity,  $t_{\text{cool}} \sim T^{\frac{1}{2}}$ .

Since we are concerned only with modelling the gas in the X-ray regime, we do not follow the cooling below  $10^5$  K. At this temperature, the gas is no longer radiating appreciably in the X-ray waveband (see Fig. 4), and may therefore (for our purposes) be ignored from further consideration. In addition, the cooling time (see Fig. 5) is becoming prohibitively short for continued computation.

If at the end of an iteration step any zone has cooled below  $10^5$  K, it is removed from subsequent analysis, and the remaining zones are adiabatically expanded to fill the vacated volume. Zones closest to the loss-site undergo the greatest degree of expansion. Conceptually, this is intended

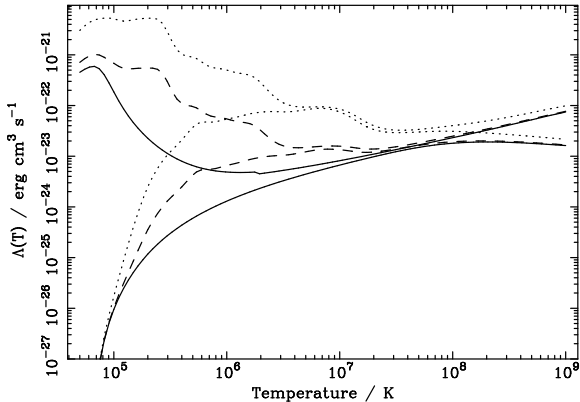


**Figure 4.** Cooling functions of plasmas of varying metallicities. He is at solar abundances in all cases. Solid – H, He only; dashed – metals at 0.3 solar abundance; dotted – metals at 3.0 solar abundance. The upper curve in each case is for all thermodynamically relevant radiation (5 eV–200 keV); the lower curve is for the X-ray wave-band 0.1–10 keV.

as a (very) crude representation of the rapid collapse of cold gas into condensed objects of negligible volume (neglecting any kind of energy injection at this point from star formation say).

### 3.4 The plasma radiation

We model the radiation coming from the plasma with the MEKAL spectral code. Thus, the abundance of the plasma becomes a relevant parameter, and each radial zone may have a different set of abundances. At the start of a simulation, spectra for each abundance set are integrated in order to obtain evaluations of the cooling function  $\Lambda(T)$ , and the cooling time integral  $\int_{T_{\min}}^T \frac{T dT}{\Lambda(T)}$  at discrete temperatures over the range of interest. The relative electron density is also calculated as a function of temperature. During the course of a simulation we interpolate amongst the tabulated values of these functions to find the value appropriate for any particular plasma temperature.

Besides these essential quantities, it is clearly of great interest to use MEKAL to produce synthetic spectra for the plasma. These calculations need not be performed at every iteration, but only when the physical state of the system is to be examined. Note that the energy range of interest is different in the two cases. In the case of  $\Lambda(T)$ , we are concerned with all the radiation that acts as a significant energy loss for the plasma over the temperature range of interest. In practice we use the energy range 5 eV–200 keV. In the case of spectra, only the much more limited wave-band of, say, 0.1–10 keV, is of relevance for comparison with the X-ray observations of *Chandra* and *XMM-Newton*. These two functions are displayed in Fig. 4. Rather than being interpolated, spectra are calculated directly for each zone.

To facilitate comparison with observations we first integrate along a line-of-sight to obtain the ‘spectral surface brightness’ at projected distance  $b$  from the centre

$$S_\nu(b) = \int_b^\infty \frac{\epsilon_\nu(r) 2r dr}{\sqrt{r^2 - b^2}}. \quad (11)$$

We then integrate again over an annulus to obtain the spec-

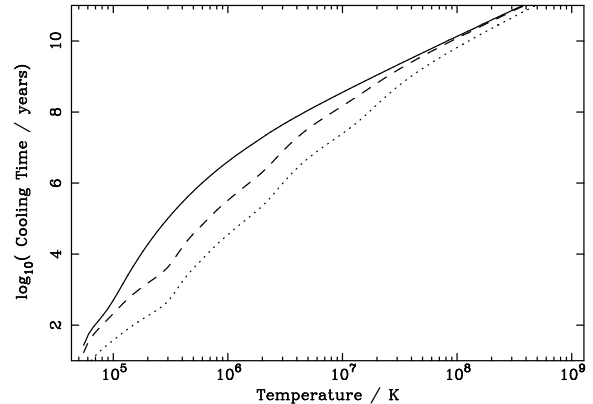


**Figure 5.** Isobaric cooling times for the plasmas of Fig. 4, calculated by integrating the total radiation curves for each abundance set. The pressure is  $10^6 \text{ K cm}^{-3}$ , with the times inversely proportional to pressure.

trum due to the (distance-weighted) contributions of all the gas along the lines-of-sight between projected radii  $b_1$  and  $b_2$

$$\begin{aligned} P_\nu(b_1 \leq b \leq b_2) &= \int_{b_1}^{b_2} db \, 2\pi b \int_b^\infty \frac{\epsilon_\nu(r) 2r dr}{\sqrt{r^2 - b^2}} \quad (12) \\ &= 4\pi[F(b_1) - F(b_2)], \quad \text{where} \\ F(b) &\equiv \int_b^\infty dr \, \epsilon_\nu(r) r \sqrt{r^2 - b^2}. \end{aligned}$$

### 3.5 The simulated observations

The integrated spectrum corresponding to each annulus is then redshifted in terms of both magnitude (as per the appropriate luminosity distance) and energy. The simulations reported here are for a redshift of 0.017, corresponding to a luminosity distance of 100 Mpc. These data are then converted to XSPEC table-model format FITS files (Arnaud 1999). For added verisimilitude we include the effects of absorption by multiplying our model spectra with the XSPEC *phabs* model, using a column density  $N_H = 10^{21} \text{ cm}^{-2}$ . Since we are now interested in spatial effects, for response matrices we have used the *Chandra* ACIS-S data, specifically the AO-2 proposal planning RMF and ARF files<sup>2</sup> for the detector aim-point position.

The simulated integration time was typically 25 ks. Noise was added via counting statistics, but no background file was included. The resulting fake data were grouped to a minimum of 20 counts per channel to ensure applicability of the  $\chi^2$  statistic.

## 4 A CHEMICALLY INHOMOGENEOUS ICM

### 4.1 A bimodal metallicity distribution

Our aim is to investigate the effects of a ‘clumpy’ metal distribution in the ICM. In our model, each radial zone corresponding to the difference equations may have a distinct

<sup>2</sup> <http://asc.harvard.edu/caldb/Aeff/>

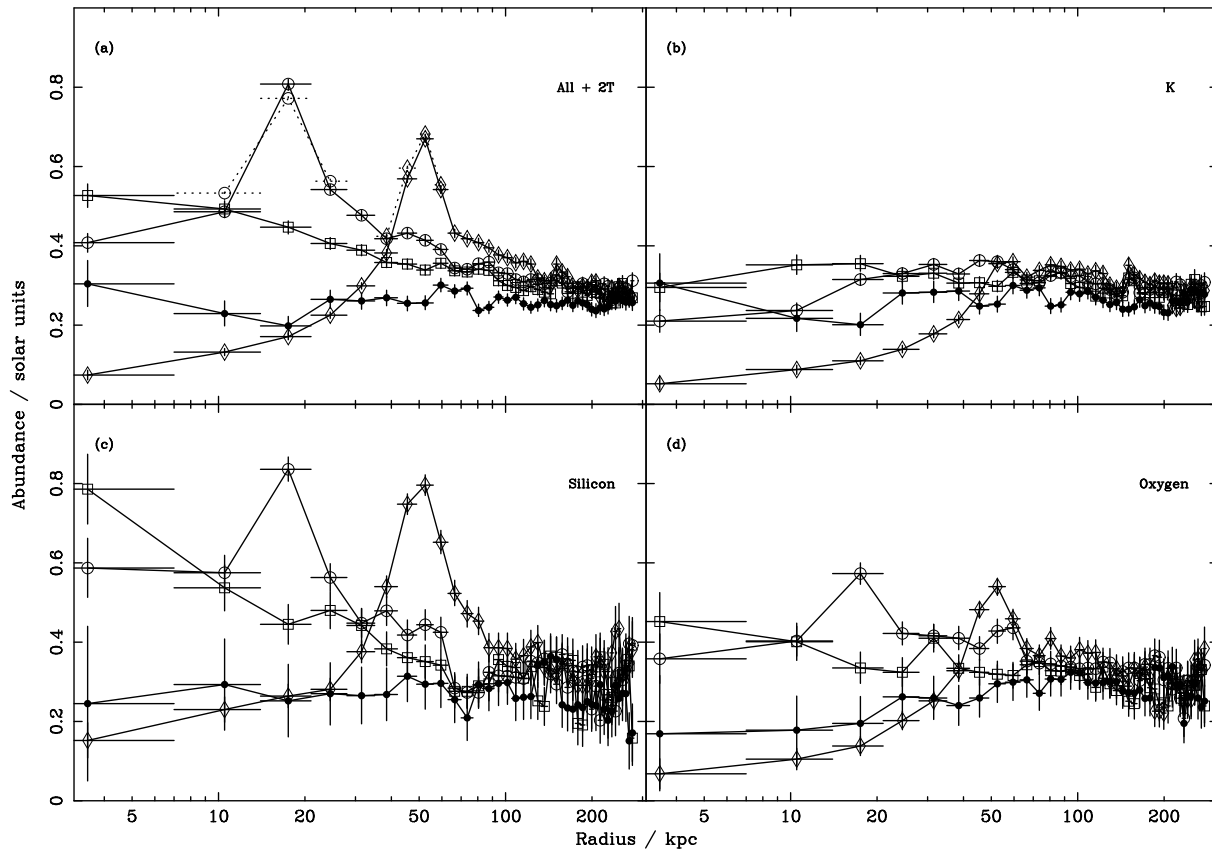


**Figure 6.** Time evolution of the observed abundance profile for a bimodal metallicity. Vertical error bars are  $1\sigma$ . See text for model properties. Filled circles – 0.0 Gyr; open squares – 1.0 Gyr; open circles – 1.2 Gyr; open diamonds – 1.6 Gyr. Unless otherwise stated, all results are for single temperature models fitted to the 0.3–7.0 keV spectral range. The simulated observation time was 25 ks for the upper two panels, and 50 ks for the lower two. Panel (a): solid lines – single temperature *mekal* fits; dotted lines – results of two temperature fits, shown where the reduced  $\chi^2$  for the single temperature fits exceeded 2.0. Panel (b): *mekal* fits to the 3.0–7.0 keV (i.e. iron K) spectral region. Panels (c) and (d): *vmekal* fits for the silicon and oxygen abundance, respectively.

set of element abundances. For this work, we have chosen one of the simplest possible inhomogeneities: 9 out of every 10 zones are taken to be pure H, He in the solar abundance ratio; whilst every tenth zone has a three times solar abundance of the 13 heavy elements included by MEKAL (with He remaining fixed at the solar value). A spatially varying distribution of this simple form appears identical to a homogeneous plasma of abundance a little less than one third solar.

Here we present the results for one particular cluster, with parameters as follows: virial temperature 8.6 keV ( $10^8$  K), which from Eqn. 9 corresponds to a virial radius of 3.4 Mpc and a halo mass of  $2.3 \times 10^{15} M_\odot$ . The radial range was modelled with 5000 zones, corresponding to a resolution of 700 pc, or around 1.5 arcsec for the redshift in question. The gas fraction was 0.17 (e.g., Ettori & Fabian 1999). With a concentration of 5, the NFW scale radius is 700 kpc, and the associated (singular isothermal sphere) velocity dispersion is  $1300 \text{ km s}^{-1}$ .

Fig. 6 illustrates the results of various XSPEC fits to the simulated observations produced for this system. We display only the central regions where cooling has progressed

significantly in the elapsed time. In each case the specified XSPEC model was multiplied with a *phabs* component. The redshift  $z$  and column density  $N_H$  were fixed at the correct values.

Panel (a) illustrates the results for single temperature *mekal* fits to the spectral range 0.3–7 keV, in which the plasma temperature, abundance and normalization were allowed to vary as free parameters.

Firstly, note that the initial fitted abundance profile is flat (within the given error bars), with no high metallicity spikes. This confirms the basic premise that a varying abundance plasma can resemble a homogeneous gas. Fig. 7 shows the evolution of the true (not fitted) temperature profile of the gas with time. Note that in the initial conditions the high metallicity zones are at higher temperatures. This is a consequence of their higher molecular weight (0.63 as opposed to 0.61 in this specific case). Recall that we require a smooth pressure profile, and that this is a function of  $T/\mu$ . These initially high temperatures are of no consequence for the subsequent evolution of the system.

As the system evolves, it is obviously apparent that the metal-rich regions cool more swiftly than the metal-poor re-

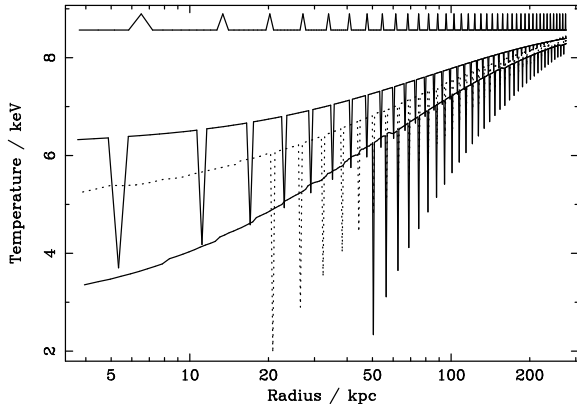


**Figure 7.** The physical temperature profiles for the model of Fig. 6. In order of decreasing average temperature, the curves are: 0.0, 1.0, 1.2 (dotted), 1.6 Gyr.

regions, leading to the rapid inversion of the ‘spikes’ in the temperature profile shown in Fig. 7. This is an inevitable consequence of the shorter cooling time of the high abundance gas (Fig. 5), which in turn is due to its enhanced radiation (Fig. 4). The cooling is naturally most extreme in the central regions where the gas density is highest, and the two-body bremsstrahlung radiation is most intense. The disappearance of the innermost spikes in the temperature profile at late times is due to the removal of the metal-rich gas from the simulation as it cools below  $10^5$  K.

This differential cooling has marked effects upon the measured abundance profile (Fig. 6a). As time passes, there is a gradual increase in the derived abundances, particularly in the central regions (for example, after 1.0 Gyr the measured value for the central abundance has risen to  $0.5 Z_{\odot}$ ). With further evolution, the central abundance begins to decrease again, leading to the situation where there is a peak in the abundance profile at an off-centre position. This peak declines in magnitude and moves outward with subsequent evolution.

This behaviour may be explained as follows. In our simulations, the metal-rich gas (contributing the emission lines) cools relatively quickly and enters the regime where line emission is more important, whereas the metal-poor gas (contributing the bulk of the continuum) cools much more slowly. The combined consequence of these two processes is an increase in the strength of the lines relative to the continuum, that is, an increase in the equivalent width of the lines. It is from the equivalent width that the fitting procedure obtains the plasma abundance. One could view this as a form of emission-weighting – as the metal-rich regions cool the intensity of their emission increases, so they increasingly dominate the spectral fits. The decrease in the central abundance at late times occurs as metal-rich gas there cools out of the X-ray regime and is lost from sight.

The maximum amplitude of the abundance peak is obviously related to the underlying spread in metallicity, but it is not obvious how one might use the former in practice to reconstruct the latter. From the theoretical point of view there is a lower limit to the extent of the variations that must exist if they are to be of any use in resolving the cooling flow problem (i.e. the lack of low-energy spectral lines). The upper limit to the spread depends on what one consid-

ers reasonable for the injection process to produce, assuming there is no active segregation of metals. Cooling time considerations also become important with extreme abundance values, if one does not wish the entire central region to become devoid of metals in the high temperature phases.

Fig. 6a also displays the results of two-temperature *mekal* fits to the data (dotted lines). These are shown only in those cases where the reduced  $\chi^2$  for the one-temperature fits was greater than 2.0. It was necessary to restrict the abundances of the two *mekal* components to be equal, there not being enough information in the spectra to obtain meaningful constraints on two individually varying abundances. Even taking this step, the values obtained for the two temperatures were more often than not very poor limits. The resulting abundances, however, agree very well with the one-temperature results.

To check that these effects are a genuine consequence of the non-uniform metal distribution, we have carried out identical simulations where all the gas has a uniform abundance of  $0.3 Z_{\odot}$ . In this case, all four abundance profiles analogous to those plotted in Fig. 6 remain resolutely flat within the errors at all times as the system evolves.

The results for lower temperature clusters (3 and 5 keV) are qualitatively similar. Obviously, with lower temperature systems there is a greater need for two-temperature models to fit the correspondingly richer spectra. Also, while for the 8 keV cluster the maximum height of the abundance peak ( $0.9 Z_{\odot}$ ) is some three times the average abundance, for the 3 keV system the peak has an amplitude roughly double the average abundance. There is less opportunity for differential cooling if the bulk of the gas begins life at lower temperatures. The evolution of lower temperature systems also takes place more rapidly (recall that from Eqn. 10 that  $t_{\text{cool}} \sim T^{\frac{1}{2}}$  for virially-scaled clusters). The general trends of behaviour are, however, the same. The small-scale metallicity variation scenario would therefore predict that the off-centre abundance peaks would be proportionately stronger in higher temperature systems.

#### 4.1.1 *Matters of resolution*

The size of the spectral annuli is controlled by two factors. Firstly, it is of course necessary to ensure that they are large enough to collect sufficient photons in a reasonable integration time to produce a meaningful signal-to-noise level. Secondly, there is also an issue of numerical resolution. The size of the annuli is such that each encompasses ten radial zones from inner to outer edge (although of course owing to projection effects each annulus receives emission from every zone whose radius is greater than that of the inner edge of the annulus). This is the minimum number necessary to avoid artificial oscillations in the fitted abundance profile, given that the fraction of metal-rich zones is 10 per cent. With a fraction  $f_{\text{hi}}$  of zones being metal rich, spectral annuli must encompass at least  $f_{\text{hi}}^{-1}$  radial zones.

Alternatively, if the spectral annuli were any smaller then we would be able to *resolve* the discrete nature of the metal distribution. Given that each annulus spans a projected radius of 7 kpc, whilst the size of the metal rich zones is 0.7 kpc, it might seem that we are claiming it would be possible to resolve the inhomogeneities with a resolution



length greater than their size. This is not the case, however, because the spatial extent of the metal-poor zones is nine times that of the metal-rich zones. When the resolution length is less than or equal to the greater of those extents, the distribution can in principle be resolved.

As is standard practice with numerical simulations, we have doubled the numerical resolution to check that the results are unaffected, and indeed they are not. This is important in this case for another reason. As well as confirming the numerical result, it illustrates just how difficult it will be to probe such metallicity distributions in real-world observations. Looked at another way, then going from the high resolution simulation to the default resolution simulation doubles the physical size scale of the metallicity variations, so that the largest relevant length scale (that of the metal-poor regions in our model) is just less than the resolution length of the spectral observations. Yet it does not do anything towards hinting that there are in fact extreme enrichment variations on just slightly smaller scales. In other words, detection of such metal variations will be an all-or-nothing affair – without adequate spatial resolution, there is no hope.

Recall as well that this is for a highly simplistic, regular, one-dimensional distribution. Given an irregular, two- or three-dimensional distribution pattern, with metal-rich ‘clouds’ drifting in and out of various lines of sight, then the problem becomes even more difficult.

If we reduce the size of the spectral annuli below the level we have used, then we do not immediately begin to resolve the correct (i.e. 0.0–3.0  $Z_{\odot}$ ) metal distribution. Instead, one begins to detect only slight variations around the mean level. These will not be significant unless one has a good quality spectrum with adequate signal-to-noise. The smaller one makes the spatial resolution element (in order to probe finer and finer regions), the larger the collecting area required in order to obtain good-quality spectra in reasonable time-scales. Good spectral resolution will also be necessary to separate the effects of the varying enrichments and allow one to constrain two-temperature models with freely varying abundances for each component. This will depend on just how extreme the metal variations are. Given that this is all for a regular, one-dimensional system, with no background file added, one can begin to appreciate the difficulties that genuine observations present in this regard.

Accepting that *direct* detection of small-scale ICM metallicity deviations will be so difficult, we are forced to consider what forms of *circumstantial* evidence it may prove possible to employ.

#### 4.1.2 Abundance gradients

Fig. 6a illustrates that a bimodal abundance distribution within a cooling flow scenario has the ability to produce an *apparent* metallicity gradient where one does not in reality exist (the real mean abundance in our simulations remains unchanged, at least until metal-rich gas begins to drop out in the inner regions). For example, consider the results after 1.0 Gyr of evolution, when the central abundance has risen to around 0.5  $Z_{\odot}$ . At later times the gradient effect would be even more pronounced if one were not able to resolve the central abundance drop.

Large-scale abundance gradients were detected in sev-

eral clusters with *ASCA* and *ROSAT*, for example: Centaurus (Fukazawa et al. 1994; Allen & Fabian 1994); Virgo (Matsumoto et al. 1996); AWM 7 (Ezawa et al. 1997); A496 (Dupke & White III 2000). The presence of an abundance gradient appears to be correlated with the existence of a cooling flow (e.g., De Grandi & Molendi 2001), although this may not be a true correlation (cooling flows generate gradients), but merely due to the mergers which disrupt cooling flows also erasing any abundance gradient. Here we have demonstrated one mechanism by which cooling flows may actually give rise to the appearance of such abundance gradients. The interplay between cooling flows and abundance gradients has been studied previously by several authors. For example, Allen & Fabian (1998) argued that it was the presence of abundance gradients in cooling flow systems that leads to the higher emission-weighted metallicities in these sources as compared to non-cooling flow clusters. Reisenegger et al. (1996) investigated the ability of cooling flows to create metallicity gradients by transport of metals.

Recently, *Chandra* studies have confirmed the presence of large-scale abundance gradients in many clusters. The unprecedented spatial resolution of *Chandra* has revealed more detail in the profiles. In several cases, clusters are found to exhibit ‘peaked’ abundance profiles (i.e. a positive radial abundance gradient in the innermost regions, coupled with a negative gradient further out), very similar to those produced in our simulations. For example: Centaurus (Sanders & Fabian 2002), where the negative abundance gradient peaks at 1.3–1.8  $Z_{\odot}$  at a radius  $\sim 15$  kpc before falling back to 0.4  $Z_{\odot}$  at the centre; A2199 (Johnstone et al. 2002), where the metallicity rises from  $\sim 0.3 Z_{\odot}$  at 200 kpc to  $\sim 0.7 Z_{\odot}$  at 30 kpc before dropping back to 0.3  $Z_{\odot}$  within the central 5 kpc; and possibly Perseus (Schmidt et al. 2002), where there may be a high metallicity ring of around 0.6  $Z_{\odot}$  at a radius of 60 kpc. It is of course intriguing when a hypothesis designed to answer one issue (lack of low temperature line emission) ends up providing a potential explanation for another (abundance gradients with off-centre peaks); though of course there is no shortage of alternative explanations for both these phenomena.

Extrapolating our results for several Gyr, one would predict that over not too long a timescale, the central region would become devoid of metals, with a ring of high metallicity at large (hence easily observable) radii that would have been detected before the *Chandra* era. This is clearly unphysical, and is easily explained away by our simple treatment of a complex problem. We start with fully formed metallicity variations rather than allowing them to develop; the variation is extreme – rather than allowing for several ‘phases’ of differing abundances we use only two, one with no metals and one with a high abundance; and we do not account for replenishment of metals through continued enrichment, which would offset the extremes of behaviour that our simple models predict.

The metallicity distribution in Perseus appears to show no correlation with the galaxies. Intriguingly, Schmidt et al. (2002) also report what may be the first signs of small-scale metallicity variations in the Perseus ICM, although the scale of the effect is at the limit of detectability with current exposure times and is not statistically significant.

A similar off-centre abundance peak is seen in the *Chandra* observation of the merging cluster A3266 (Henriksen

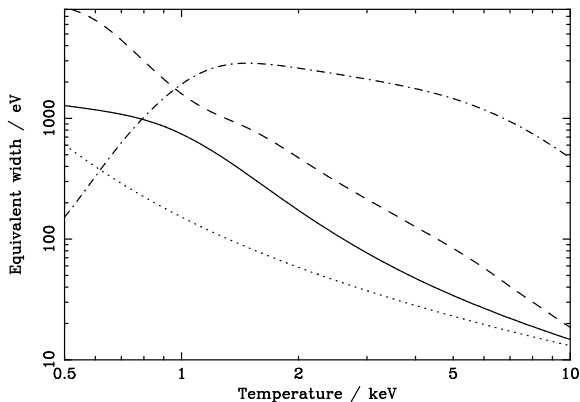


**Figure 8.** The temperature dependence of the equivalent widths for various ICM plasma spectral lines, for a solar metallicity plasma. Dot-dashed iron K; dashed iron L; dotted oxygen K; solid silicon K. See text for details.

& Tittley 2002). These authors suggest an alternative explanation for this feature involving the merging subcluster depositing enriched gas close to the centre of the cluster. Shock heating is then called upon to preferentially deplete the enriched region of the lightest, most mobile elements, H and He, so that the metallicity may be increased without an associated raising of the density, for which there is no observational evidence. This explanation requires efficient motion of ions, something which it is not clear can happen even if conduction is relatively unimpeded. Moreover, these efficient transport properties are required precisely in the regions where subcluster merging is taking place. Cold-fronts (see Section 5) are plausible evidence that transport properties may be highly suppressed in such volumes, presumably due to separate magnetic structures existing in the merging components. It is intriguing that off-centre abundance peaks appear to be found both in clusters with and without cooling flows. If we are looking at the same phenomenon in both cases (this of course by no means clear), and if a common mechanism is responsible, this would suggest that it is something associated with neither the cooling flow process, nor the merger process.

#### 4.1.3 Equivalent width effects

The original *ASCA* abundance gradients were clearly detected in the equivalent width of the iron K line (e.g. in Centaurus where Fukazawa et al. 1994 report an increase by a factor of three on moving to the central regions of the cluster). Excluding the iron L complex from the *Chandra* data for Centaurus by simply fitting to the high-energy end of the spectrum (3–7 keV), whilst obviously increasing the noise, does not affect the qualitative nature of the conclusions regarding the abundance profile (Sanders & Fabian 2002). Fitting our model spectra just using the data in this region produces different results, however, as illustrated in Fig. 6b. The noise level has increased somewhat, but the qualitative behaviour has also altered. There is still something of an initial increase in the central abundance at early times, leading once again to the generation of an apparent gradient. At later times, however, the highly peaked abundance profile that was present when fitting to the entire

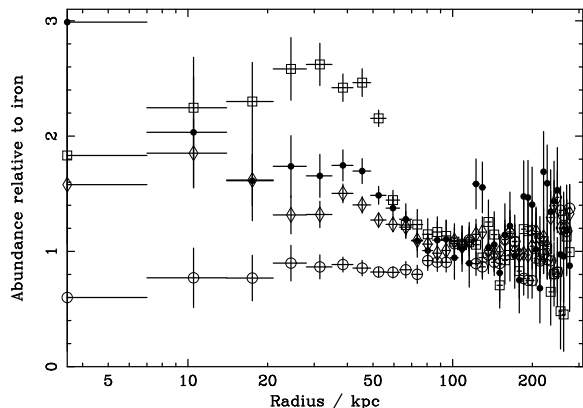


**Figure 9.** Ratios of element abundance to that of iron. Results are for the last of the times plotted in Fig. 6. Filled circles – magnesium; open squares – neon; open circles – oxygen; open diamonds – silicon.

spectrum does not appear. Instead the central abundance merely dies away. Excluding the iron K lines, however, by fitting only to the spectra between 0.3–5 keV produces much the same results as using the entire spectrum.

Thus there is a qualitative difference in behaviour when fitting to the iron K lines as compared to the iron L lines that must be explained. In Fig. 8 we illustrate the temperature dependence of the equivalent width for various important ICM spectral lines, calculated from *MEKAL* spectra.

Consider just the results for the iron. Upon cooling from high temperatures, the equivalent width of the iron K lines increases somewhat, then rapidly dies away below 1 keV. The width of the L complex, on the other hand, increases strongly and monotonically as the temperature decreases. Consequently, with a bimodal metallicity, the strength of the iron K lines relative to the continuum increases to a relatively small extent on cooling, producing the initial slight increase in the central abundance, before dying away as cooling progresses. The strong monotonic increase in the iron L width with cooling produces a much greater change relative to the continuum.

To illustrate this point further, the equivalent widths for the silicon and oxygen K lines are also plotted in Fig. 8. Both increase monotonically as the temperature is reduced, but the rate of change for oxygen is relatively small, whereas silicon shows very similar behaviour to iron L. The arguments of the previous paragraph are borne out by the results of *vmekal* fits to the model spectra (Figs. 6c and d show the fits for silicon and oxygen respectively). The qualitative behaviour of both profiles is the same, but the oxygen profile shows a less pronounced peak.

In Fig. 9 we plot the ratio of element abundance to iron abundance (both in solar units), for various elements, for the last of the times illustrated in Fig. 6. Neon and magnesium (and to a lesser extent silicon) appear overabundant, whilst oxygen appears slightly underabundant.

## 4.2 Genuine abundance gradients

Given that flat metallicity profiles coupled with bimodal distributions are unable to fully reproduce the observed abun-

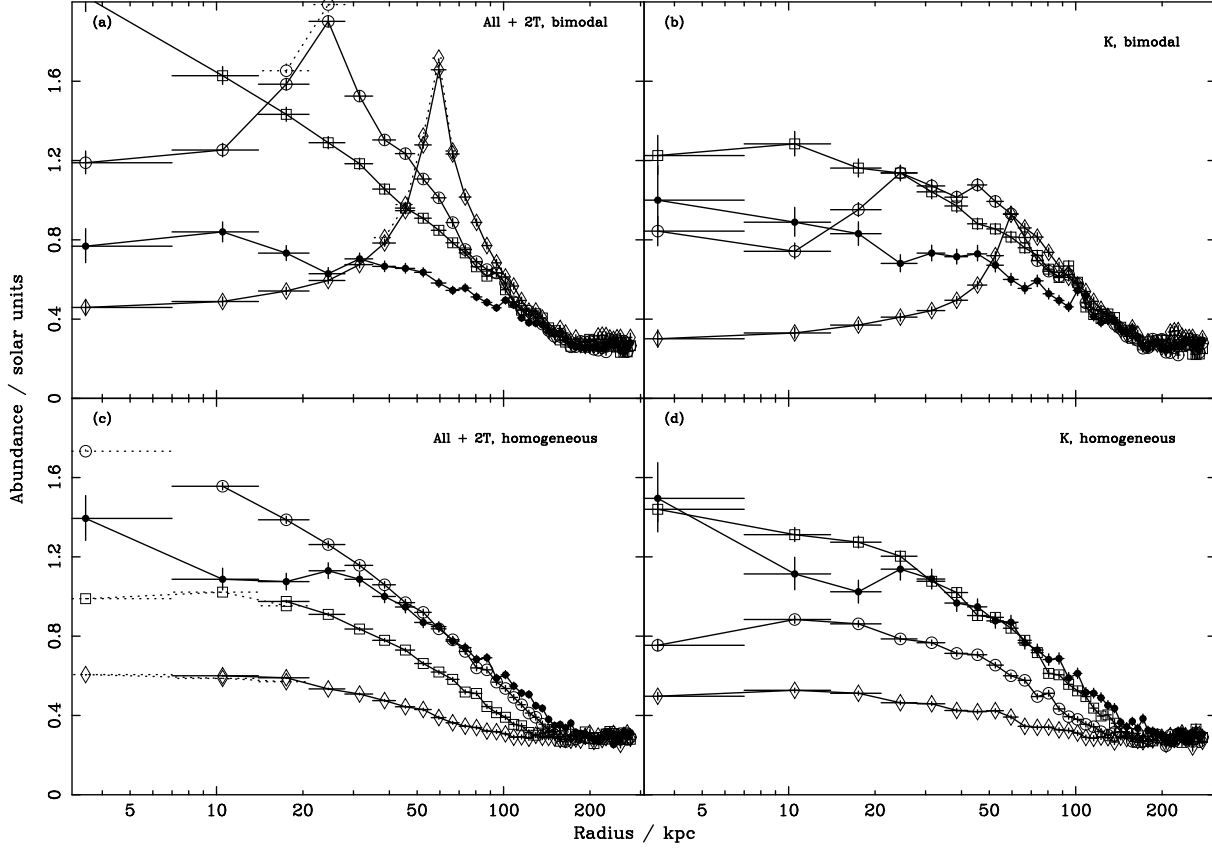


**Figure 10.** Time evolution of the observed abundance profile for clusters with genuine abundance gradients. Vertical error bars are  $1\sigma$ , simulated observation time 25 ks, all results for single temperature *mekal* models unless otherwise stated. Top two panels, bimodal metal distribution: filled circles – 0.0 Gyr; open squares – 0.4; open circles – 0.5; open diamonds – 0.8. Bottom two panels, homogeneous metal distribution: filled circles – 0.0 Gyr; open squares – 1.3; open circles – 2.5; open diamonds – 3.8. Left-hand panels: fits to 0.3–7.0 keV region, dotted lines show results from two temperature fits where the reduced  $\chi^2$  for the single temperature fits exceeded 2.0. Right-hand panels: fits to the 3.0–7.0 keV (i.e. iron K) spectral region.

dance trends, we have considered also clusters with genuine gradients in their abundance profiles. We have parameterized the profile in the following manner:

$$Z(r) = \begin{cases} \bar{Z} + (Z_c - \bar{Z}) \left(1 - \frac{r}{r_0}\right)^n & r < r_0 \\ \bar{Z} & r \geq r_0 \end{cases} \quad (n \geq 0) \quad (13)$$

where  $\bar{Z} = 0.3$  is the mean cluster abundance;  $Z_c = 2.0$  is the central abundance;  $r_0 = 200$  kpc is the extent of the gradient; and  $n = 1.5$  controls its severity.

We have carried out simulations both with homogeneous metallicities (i.e. the distribution smoothly follows the profile), and with a bimodal behaviour similar to before (i.e. 90 per cent of the gas is metal-poor, the other 10 per cent has ten times the abundance dictated by Eqn. 13). The results are displayed in Fig. 10. Once again, the bimodal system develops an off-centre abundance peak, of a larger amplitude than before. This time, the trend is reproduced when fitting solely to the high-energy part of the range, panel (b). In the homogeneous system, on the other hand, no such peak develops, rather the abundance declines reasonably smoothly back down towards a flatter state. Note that the temporal

evolution is in both cases faster, owing to the higher abundances that are present.

### 4.3 Cooling flow equivalent widths

We have used simulations similar to those described in the previous section to produce synthetic *XMM-Newton* RGS spectra in order to investigate in more detail the ideas of Section 2 on the suppression of the low-temperature lines. These broadly reproduce the same results as the isobaric model, Eqn. 3. They do reveal another factor, however, which conspires to reduce the line suppression. When geometrical (i.e. position within the cluster potential) considerations are taken into account, the metal-rich gas always has a larger cooling radius at any instant than the metal-poor gas, as a fairly obvious consequence of its faster cooling rate. In the case of an 8.6 keV cluster, for example, where 10 per cent of the gas is made to be metal-rich, the fraction of cooled mass originating from the enriched phase asymptotes to about 1/8, rather than 1/10. This reduces still further the equivalent width suppression we can expect from a bimodal distribution of metals.

## 5 DISCUSSION

To address the question of how small-scale ICM abundance variations might come about, supernovae can be considered as essentially point sources (on ICM scales) of extremely high metallicity gas. In of themselves, these have structures that are far from simple (e.g., Hughes et al. 2000). One way in which escape of the enriched gas from the potential well of the host galaxy into the ICM may occur is via superwinds (e.g., Heckman 2001) (although other processes such as ram-pressure stripping and pregalactic winds are doubtless significant). Superwinds have a complex, multiphase structure in which it is difficult to probe directly the energetic, enriched gas driving the wind. There is, however, clear evidence for complicated structure in the wind on very small scales in the optical and soft X-ray (e.g., Strickland 2001). In our opinion, the question ought to be posed the other way around: how might the ICM become uniformly enriched?

There are essentially two issues that determine whether or not the situation as we have chosen to model it is physically realistic: i) how are the metals injected into the ICM, and ii) once in the ICM, do the metals move to spread out over a wide area or remain confined? The answers to both these questions remain uncertain at present. To address the second question first, following Spitzer (1962), we may express the deflection time (average time for a cumulative deflection of  $90^\circ$ ) for particles of mass  $m$ , charge  $Ze$  diffusing through field particles of mass  $m_f$ , charge  $Z_f e$ , density  $n_f$  as

$$\tau = \frac{6\sqrt{3}\pi\epsilon_0^2 k_B^{3/2}}{e^4} \frac{m^{1/2} T^{3/2}}{Z^2 Z_f^2 n_f \mathcal{F}(x) \ln \Lambda} \quad (14)$$

where

$$x = \sqrt{\frac{3m_f}{2m}} \quad (15)$$

$$\mathcal{F}(x) \equiv \operatorname{erf} x + \frac{d}{dx} \left( \frac{\operatorname{erf} x}{2x} \right) \quad (16)$$

with  $\operatorname{erf}$  the standard error function,  $\ln \Lambda$  the Coulomb logarithm, and assuming that all species are in thermal equilibrium at temperature  $T$ . The factor  $\mathcal{F} \leq 1$  is the Chandrasekhar correction for the finite mass of the field particles.

Numerically

$$\tau \approx 0.26 \text{ Myr} \quad A^{1/2} \left( \frac{T}{10^8 \text{ K}} \right)^{3/2} \left( \frac{n_f}{\text{cm}^{-3}} \right)^{-1} \frac{1}{Z^2 Z_f^2 \mathcal{F} \ln \Lambda} \quad (17)$$

with  $A$  the test particle mass in units of the proton mass.

As was shown by Rephaeli (1978) for the case of sedimentation, in the ICM the contributions from field particles other than protons (particularly helium nuclei) are significant. Summing over the elements in a  $0.3 Z_\odot$  plasma with iron nuclei as test particles, we find that  $\tau$  is reduced by around a factor of two from the value for a pure proton plasma. At  $10^8 \text{ K}$ , and with  $n_H = 10^{-3} \text{ cm}^{-3}$ , we find the corrected deflection times for iron and helium nuclei are  $\tau_{\text{Fe}} \approx 0.3 \text{ Myr}$ ,  $\tau_{\text{He}} \approx 4 \text{ Myr}$ .

From standard kinetic theory, the root-mean-square three-dimensional distance a particle will diffuse in a time  $t$  is given by

$$r_{\text{rms}} = \sqrt{2\lambda v_{\text{rms}} t} = v_{\text{rms}} \sqrt{2\tau t} = \sqrt{\frac{6k_B T \tau t}{m}}, \quad (18)$$

where  $\lambda = \tau v_{\text{rms}}$  is the mean free path. Hence we can esti-

mate that iron nuclei may diffuse about 20 kpc in 1 Gyr. To maintain small-scale abundance variations over significant timescales in the ICM, we therefore require a strong suppression of diffusion. This result is to be expected, as it is equivalent to the strong suppression of conduction that has traditionally been invoked for the multiphase cooling flow picture. Magnetic fields have normally been appealed to as the causative agent to dampen transport properties in an ionized gas. Early calculations (e.g., Tribble 1989) appeared to show that a tangled magnetic field would indeed produce a strong reduction in transport. More recent calculations considering a chaotic field with turbulence extending over a wide range of length scales indicate that the suppression may in fact be minimal (Narayan & Medvedev 2001).

In practice, simple diffusion is probably unlikely to be the limiting factor for the spread of ICM metals. Convection, turbulence due to radio sources, galactic wakes, etc., will also play roles to varying degrees. If, however, the abundance drops observed with *Chandra* in the central regions of the ICM for several clusters are genuine, then this will imply limits on the amount of convection or mixing that can have taken place (else these features would have been smoothed out). It does not seem unreasonable to explore some of the consequences of small-scale metallicity variations, and to keep the possibility in mind during spectral analyses.

The question as to whether or not the metals in the intracluster and intergalactic media are homogeneously distributed remains an open one. There is a non-negligible scatter in Galactic stellar metallicities for stars of all ages (the scatter increases for low metallicity stars), which has been taken to suggest that that Galactic disc has been chemically inhomogeneous throughout its development (e.g., McWilliam 1997). Classical galactic chemical evolution models have tended to assume instantaneous dispersion of synthesized elements.

The average metallicity of the intracluster medium on large scales has for some time been reasonably well established at roughly  $1/3$  solar in most cases, both for nearby (Edge & Stewart 1991) and distant (Mushotzky & Loewenstein 1997) clusters. Until comparatively recently, however, there has been little information on how the ICM metals might be distributed on finer scales. There is, in our opinion, no particular reason why the whole ICM should be uniformly enriched to the same metallicity, although this might be one's natural assumption. As we discuss in Section 4.1.1, direct detection of small-scale abundance variations in the ICM will be very difficult. Consequently, we feel it is impossible to rule out such variations at the present time.

Recently, a deal of support has been given to the idea that thermal conduction might be operating in cluster cores at significant levels (e.g., Narayan & Medvedev 2001; Voigt et al. 2002; Fabian et al. 2002). Whilst this runs contrary to the established multiphase cooling flow picture (Nulsen 1986), it seems to have a degree of success in matching the observed temperature profiles. It is certainly the case, though, that at least in some regions of the ICM, conduction is highly suppressed. This is revealed by the 'cold-fronts' seen in several cluster cores, e.g. A2142 (Markevitch et al. 2000). It was shown by Ettori & Fabian (2000) that such features, which correspond to a sharp jump in the surface brightness profile, indicate a strong (factors of several hun-

dred) *local* suppression of the thermal conductivity, else the temperature discontinuity that is responsible for the brightness jump would be quickly washed out. If thermal conduction is suppressed, then ion movement must be even more restricted, since net heat conduction may still take place without individual electrons travelling a significant distance. If thermal conduction is operating with a degree of efficiency, however, then the same need not necessarily apply to ion motion. If this were the case, though, there would be the possibility of sedimentation of the heavy elements (Fabian & Pringle 1977; Rephaeli 1978; Fabian et al. 2002). Cold-fronts of course only provide direct evidence for inhibited thermal conduction across the fronts themselves. It is possible (though as yet far from proven) that conduction may reach the Spitzer (1962) value elsewhere (e.g., Voigt et al. 2002). If conduction is operating efficiently, it does not necessarily rule out small-scale metallicity variations, but it does weaken the case, both from the point of view of reducing/removing the motivation for them (suppressing the low-temperature cooling flow line emission by suppressing the low temperature gas), and by making it less likely that such conditions can persist.

Our modelling is simplistic, and it may be argued that the conditions as we have chosen to represent them are not physically relevant. For example, there is no possibility of segregation of elements based on weight (that is, it is not possible for the metal-rich gas to sink to the centre). This is a consequence of our adopting the theoretical framework of Nulsen (1986), which requires that in a multiphase flow the various phases co-move, i.e. there is a single velocity profile. The arguments for this idea are set out in detail in Nulsen (1986). Also, the timescale over which the changes in the abundance profile occur is somewhat short. This is a result of the rather unphysical initial condition; starting out with regions enriched to  $3Z_{\odot}$  and not allowing any replacement of cooling metals. A more realistic treatment would allow the metallicity to build up initially with time and then allow for some replenishment, and possibly also for different distributions of SNe Ia and II products. However, we are not concerned here with producing detailed models of the evolution, but rather in seeing what the general trends of behaviour might be. Note that because we have restricted our attention to single-phase models, there is no real transport of material by the cooling flow, since all the mass loss (except for the metal-rich zones) takes place in the centre. Reisenegger et al. (1996) demonstrated the ability of multiphase cooling flows to create (genuine) abundance gradients through transport of injected materials. Thus we may expect that a more sophisticated multiphase treatment of this process might reveal more complex effects.

Given that the abundance gradients observed with *ASCA* and *Chandra* are seen clearly in the iron K line, the results of Section 4.1.3 imply that this cannot be solely due to a bimodal distribution of metallicities. The results are not, however, inconsistent with such a metal distribution, at least in the simple scenario outlined here. At the very least, we have presented another reason to be wary of the iron L complex when fitting to X-ray spectra (e.g., Finoguenov et al. 2000). In our case, it is not due to the complex atomic physics of the L shell (the code we use to generate the spectra is the same as that we use to fit them), but rather to the temperature dependence of the equivalent width. Recall

that iron is really the only ICM element for which one has two strong spectral indicators (K and L); for other elements only the K lines are useful. Playing devil's advocate, one could therefore imagine a situation in which the observed gradients in the *iron* profile are genuine, but those in the other elements are due to a process such as the one outlined here. This would, for example, severely impact on estimates of the SNe Ia:II importance ratio. Of course, this simple model would not explain the matching radial scales of the variations for iron and the other elements in this case. Nor could it explain any correlation between the iron profile and the visible light in the central regions of the cluster.

Another process which may give rise to the same sort of radial abundance profile as those seen here (namely a peak in the abundance at an off-centre position) is resonant scattering (Gil'fanov et al. 1987). This acts to redistribute photons from the central regions of the cluster (where the optical depth is highest) to a surrounding ring. See the work of Mathews et al. (2001) for an application of these ideas to M87. Computation of detailed optical depths requires knowledge of the velocity structure of the gas along the line of sight. We will not comment on the resonant scattering issue here, except to say that to some extent the ideas of this paper and those of resonant scattering are in conflict. As was pointed out by Wise & Sarazin (1992), clumping of the ICM reduces the amount of scattering that takes place. X-ray surface brightness profiles depend on the rms density  $\sqrt{\langle n^2 \rangle}$ , whereas electron scattering depends on the mean density  $\langle n \rangle$ . The rms of a set of numbers is always greater than their mean (unless the numbers are all equal). Thus increasing the degree of clumping in the plasma reduces the mean density relative to the rms density and so reduces the relative effect of scattering.

Another possibility is that the 'extra' metals in the central regions of many clusters are to be associated with the central cD galaxy. Makishima et al. (2001) have suggested an alternative explanation for the enhanced emission seen at the centre of many clusters, which has traditionally been attributed to the cooling flow phenomenon by many researchers. Instead, these authors suggest the excess may be associated with the *interstellar* medium of the central cD galaxy. One argument invoked against the cooling flow interpretation is the fairly frequent presence of metallicity increases near cluster centres. Our present work suggests a mechanism by which such effects may indeed be produced by cooling flows. The reality or otherwise of any central dips in abundance would be an important discriminant for these two interpretations.

Böhringer et al. (2002) also give some consideration to the possible effects of inhomogeneous metallicities on the observed abundances (section 2.2 of their paper). Unlike our consideration of individual emission lines, they look at the overall observed metallicity of the spectrum, as inferred from the global ratio of power in all emission lines to power in the continuum. These authors also discuss some comparisons between the shape of the spectrum around the 1 keV region for M87 and the predictions of the bimodal model. All hypotheses live or die through comparison with data, so such investigations are highly necessary, but there is a large parameter space to investigate. And as they point out, such checks must be made on a source-by-source basis. They find a poor fit between the actual spectral shape and the pre-

dictions of the bimodal hypothesis (e.g. their fig. 6). Note, however, that this is for the case where the normalizations of the metal-rich and metal-poor phases are ‘roughly equal’. We would not expect such a division to be successful in reducing the EW of the low temperature lines by an appreciable amount.

Our main result is that the observed equivalent width suppression for low temperature emission lines in a cooling flow spectrum due to a metal distribution which is inhomogeneous on small-scales is not as great as one might expect. For example, if all the metals are concentrated in 10% of the gas, the suppression of the low-temperature lines relative to those from high temperature gas is only about a factor of 3 (Section 2.2.2). It seems unlikely, therefore, that this method in isolation could produce a reduction in equivalent width equal to that seen in data, without pushing the bimodality of the metal distribution to extreme levels. There is an effect, but it is not large enough. We have also shown that small-scale metallicity variations can give rise to interesting effects in the observed abundance profiles (Section 4.1.2) as compared to the true profiles. Such effects would give rise to serious difficulties in terms of interpreting abundances in cluster central regions. The possibility of small-scale metallicity variations ought to be borne in mind when analysing high resolution X-ray spectra of cluster central regions.

## ACKNOWLEDGMENTS

We thank PPARC (RGM) and the Royal Society (ACF) for support. RGM is grateful to Steve Allen and Enrico Ramirez Ruiz for useful suggestions, and to Robert Schmidt for many helpful discussions.

## REFERENCES

- Allen S. W., 2000, MNRAS, 315, 269  
 Allen S. W., Fabian A. C., 1994, MNRAS, 269, 409  
 Allen S. W., Fabian A. C., 1998, MNRAS, 297, L63  
 Anders E., Grevesse N., 1989, *Geochim. Cosmochim. Acta*, 53, 197  
 Arnaud K. A., 1999, OGIP Memo, 92-009  
 Böhringer H., Matsushita K., Churazov E., Ikebe Y., Chen Y., 2002, A&A, 382, 804  
 Brickhouse N. et al., 1995, *Legacy*, 6, 4  
 Bullock J. S., Kolatt T. S., Sigad Y., Somerville R. S., Kravtsov A. V., Klypin A. A., Primack J. R., Dekel A., 2001, MNRAS, 321, 559  
 Cole S., Lacey C., 1996, MNRAS, 281, 716  
 De Grandi S., Molendi S., 2001, ApJ, 551, 153  
 Dupke R. A., White III R. E., 2000, ApJ, 537, 123  
 Edge A. C., Stewart G. C., 1991, MNRAS, 252, 414  
 Ettori S., Fabian A. C., 1999, MNRAS, 305, 834  
 Ettori S., Fabian A. C., 2000, MNRAS, 317, L57  
 Evrard A. E., Metzler C. A., Navarro J. F., 1996, ApJ, 469, 494  
 Ezawa H., Fukazawa Y., Makishima K., Ohashi T., Takahara F., Xu H., Yamasaki N., 1997, ApJ, 490, L33  
 Fabian A. C., 1994, ARA&A, 32, 277  
 Fabian A. C., Mushotzky R. F., Nulsen P. E. J., Peterson J. R., 2001, MNRAS, 321, L20  
 Fabian A. C., Pringle J. E., 1977, MNRAS, 181, 5P  
 Fabian A. C., Voigt L. M., Morris R. G., 2002, MNRAS, 335, L71  
 Finoguenov A., David L. P., Ponman T. J., 2000, ApJ, 544, 188  
 Fukazawa Y., Ohashi T., Fabian A. C., Canizares C. R., Ikebe Y., Makishima K., Mushotzky R. F., Yamashita K., 1994, PASJ, 46, L55  
 Gil’fanov M. R., Syunyaev R. A., Churazov E. M., 1987, *Pis’m’a Astron. Zh.*, 13, 7  
 Heckman T. M., 2001, in Mulchaey J., Stocke J., ed, *Extragalactic Gas at Low Redshift*. ASP Conf. Ser. (astro-ph/0107438)  
 Henriksen J. R., Tittley E. R., 2002, ApJ, accepted (astro-ph/0207063)  
 Hughes J. P., Rakowski C. E., Burrows D. N., Slane P. O., 2000, ApJL, 528, L109  
 Iwasawa K., Fabian A. C., Allen S. W., Ettori S., 2001, MNRAS, 328, L5  
 Johnstone R. M., Allen S. W., Fabian A. C., Sanders J. S., 2002, MNRAS, in press  
 Johnstone R. M., Fabian A. C., Edge A. C., Thomas P. A., 1992, MNRAS, 255, 431  
 Kaastra J. S., Ferrigno C., Tamura T., Paerels F. B. S., Peterson J. R., Mittaz J. P. D., 2001, A&A, 365, L99  
 Kaastra J. S., Mewe R., 1993, *Legacy*, 3, 16  
 Makishima K. et al., 2001, PASJ, 53, 401  
 Markevitch M. et al., 2000, ApJ, 541, 542  
 Mathews W. G., Buote D. A., Brighenti F., 2001, ApJ, 550, L31  
 Matsumoto H., Koyama K., Awaki H., Tomida H., Tsuru T., Mushotzky R., Hatsukade I., 1996, PASJ, 48, 201  
 McWilliam A., 1997, ARA&A, 35, 503  
 Mewe R., Kaastra J. S., Liedahl D. A., 1995, *Legacy*, 6, 16  
 Molendi S., Pizzolato F., 2001, ApJ, 560, 194  
 Mushotzky R. F., Loewenstein M., 1997, ApJ, 481, L63  
 Narayan R., Medvedev M. V., 2001, ApJ, 562, L129  
 Navarro J. F., Frenk C. S., White S. D. M., 1997, ApJ, 490, 493  
 Nulsen P. E. J., 1986, MNRAS, 221, 377  
 Peterson J. R., Ferrigno C., Paerels F. B. S., Kahn S. M., Jernigan J. G., Bleeker J. A. M., Tamura T., 2002, in Jansen F., ed, *New Visions of the X-Ray Universe in the XMM-Newton and Chandra era*. ESA SP-488 (astro-ph/0202108)  
 Peterson J. R. et al., 2001, A&A, 365, L104  
 Reisenegger A., Miralda-Escude J., Waxman E., 1996, ApJ, 457, L11  
 Rephaeli Y., 1978, ApJ, 225, 335  
 Sanders J. S., Fabian A. C., 2002, MNRAS, 331, 273  
 Schmidt R. W., Fabian A. C., Sanders J. S., 2002, MNRAS, accepted (astro-ph/0207290)  
 Spitzer L., 1962, *Physics of Fully Ionized Gases*. Wiley  
 Strickland D., 2001, in Matteucci F., Fusco-Femiano R., ed, *Chemical Enrichment of Intracluster and Intergalactic Medium*. ASP Conf. Ser., p. 387  
 Tamura T. et al., 2001, A&A, 365, L87  
 Thomas P. A., 1988, MNRAS, 235, 315  
 Tribble P. C., 1989, MNRAS, 238, 1247  
 Voigt L. M., Schmidt R. W., Fabian A. C., Allen S. W., Johnstone R. M., 2002, MNRAS, 335, L7  
 Wise M. W., Sarazin C. L., 1992, ApJ, 395, 387